

Spin stiffness and topological defects in two-dimensional frustrated spin systems

Michel Caffarel,¹ Patrick Azaria,² Bertrand Delamotte,³ and Dominique Mouhanna³

¹CNRS–Laboratoire de Chimie Théorique, Université Pierre et Marie Curie, 4 Place Jussieu, 75252 Paris, France

²CNRS–Laboratoire de Physique Théorique des Liquides, Université Pierre et Marie Curie, 4 Place Jussieu, 75252 Paris, France

³CNRS–Laboratoire de Physique Théorique et Hautes Energies, Université Pierre et Marie Curie, Université Denis Diderot, 4 Place Jussieu, 75252 Paris, France

(Received 20 December 2000; published 12 June 2001)

Using a *collective* Monte Carlo algorithm we study the low-temperature and long-distance properties of two systems of two-dimensional classical tops. Both systems have the same spin-wave dynamics (low-temperature behavior) as a large class of Heisenberg frustrated spin systems. They are constructed so that to differ only by their topological properties. The spin stiffnesses for the two systems of tops are calculated for different temperatures and different sizes of the sample. This allows one to investigate the role of topological defects in frustrated spin systems. Comparisons with renormalization group results based on a nonlinear sigma model approach and with the predictions of some simple phenomenological model taking into account the topological excitations are done.

DOI: 10.1103/PhysRevB.64.014412

PACS number(s): 75.10.Hk, 05.10.Ln, 11.10.Hi, 11.10.Lm

I. INTRODUCTION

The long-distance behavior of the classical Heisenberg antiferromagnet on a triangular lattice (HAFT) model has been the subject of much interest. In three dimensions a most important issue is the nature of the universality of its phase transition.^{1–7} In two dimensions, this model has also been widely studied since it exhibits a nontrivial finite-temperature behavior due to the presence of topological excitations. Topology enters the problem since the order parameter of the model belongs to $SO(3)$ whose first homotopy group is $\pi_1[SO(3)] = Z_2$. As a consequence, there exist topologically stable point defects — called vortices — for this two-dimensional system. Arguments involving entropy and energy of the defects suggest the occurrence of a change of behavior at a finite temperature T_V between a pure spin wave regime with confined vortices for $T < T_V$ and a regime of free vortices for $T > T_V$. Several Monte Carlo studies of the HAFT model^{8–11} and of some generalizations with an easy-axis exchange anisotropy^{12–14} have indeed revealed the existence of various regimes resulting from the presence of defects.

Here, our purpose is to shed some light on the interplay between vortices and spin waves in two dimension (2D) by studying with Monte Carlo simulations two lattice models of ferromagnetically interacting tops. Both models have the *same* spin-wave dynamics as the original HAFT model but they differ by their topological properties: the first one has the same topological content as the HAFT model, the second one is topologically trivial. The role played by the topological defects emerges from the comparison between these two models. Note that this comparative study would have been more difficult to implement directly on the original HAFT model. The physical quantity we consider in our study is the spin stiffness which, for a spin system on a finite lattice of size L , measures the free-energy increment resulting from a twist of the boundary conditions.^{15,16} The spin-wave part of the spin stiffness identifies with the coupling constant of the nonlinear sigma ($NL\sigma$) model renormalized at scale L by

thermal fluctuations. Accordingly, the behavior of the spin stiffness as a function of the size of the lattice provides a direct test of the perturbative renormalization group (RG) predictions of the $NL\sigma$ model. For the models of tops studied here we expect that, at sufficiently low temperature — for T significantly smaller than T_V — where the physics is dominated by pure spin waves, the behavior of the spin stiffnesses agrees with the RG predictions. On the other hand, we also expect that, for a topologically nontrivial model, near T_V , the vortices also contribute to the spin stiffness. For such a model the behavior of the spin stiffness must disagree with the standard RG predictions. One great advantage of the spin stiffness ρ is that, in contrast with the correlation length ξ which cannot be easily computed at very low temperature since it diverges typically as $\exp(1/T)$, ρ has a smooth behavior at low temperature. It is thus, in principle, easily computable. Regarding Monte Carlo simulations, a central aspect is that, at the low temperatures we are interested in, the dynamics of 2D spin systems is governed by strongly correlated spin waves, independently of the presence of vortices. These modes are responsible for a severe critical slowing down which makes difficult the convergence of simulations based on local algorithms in which one spin is flipped at each Monte Carlo step (“local update” Monte Carlo schemes). To resort to collective algorithms based on global updates (construction of clusters) is then important.^{17,18} However, as is well known, such algorithms work well for ferromagnetic systems but not for frustrated ones. Note that together with the ability of comparing topologically different models, this aspect is an additional motivation to consider ferromagnetic top models rather than the original HAFT one. Actually, the implementation of the basic rules of collective algorithms for systems consisting of tops is itself not so clear. However, this difficulty can be circumvented by rewriting the models of tops considered here as ferromagnetic four-component spin systems while, of course, preserving both their spin-wave and topological contents. Thanks to these various tricks and to the cluster algorithm we are then able to scan a large temperature range below T_V while fully controlling the convergence of our simulations. It should be noted that previous Monte Carlo calculations of the spin stiffness on related

models (HAFT model and generalizations) have been done by using Monte Carlo schemes with local updates.^{8–13} Note that, in contrast with these works, we have considered here very small temperatures, $T \ll T_V$. To resort to a nonlocal algorithm to accelerate the convergence of simulations is therefore essential. Note also that at the intermediate temperatures where the necessity of using global Monte Carlo schemes is less important we have also found a clear improvement associated with the use of cluster algorithms.

The main result of this paper is that we have found some striking differences in the behavior of the spin stiffnesses as a function of the linear size for the two models, with and without topological excitations. At very low temperatures the temperature-rescaled spin-stiffness $\tilde{\rho} = \rho/T$ (the natural quantity to consider, see below) of both models displays the characteristic behavior:

$$\tilde{\rho} = \frac{\rho}{T} \sim \frac{1}{4\pi} \ln \frac{\xi}{L} \quad (1)$$

predicted by the perturbative RG approach of the NL σ model.¹⁶ This is, of course, expected since the spin-wave contents of both models are identical. We call the regime corresponding to this range of temperatures the “spin-wave” regime. Note that, for one value of the temperature, this asymptotic scaling of $\tilde{\rho}$ with respect to $\ln L$ has already been confirmed directly on the HAFT model by Southern and Young.⁹ At higher, but still low, temperatures the two models begin to display different behaviors. While the spin stiffness of the topologically nontrivial model still displays the previous characteristic behavior, its absolute magnitude with respect to the trivial model is found to decrease quite rapidly as a function of the temperature. We propose to refer to this regime as an “almost-spin-wave” regime, a regime where the only significant effect of vortices is just to shift down the value of ρ/T . Next, at higher temperatures we enter a regime called here the “vortex” regime where the vortices play a major role. In this regime, the spin stiffness loses its regular behavior. It exhibits large fluctuations around its mean value with the presence of “plateaux” and abrupt jumps as a function of the linear size. Nevertheless, by considering the global behavior of the curve it is still possible to define some effective linear regime as a function of $\ln L$ similar to that described by Eq. (1). However, in contrast with the spin-wave regime, the slope of the spin stiffness is no longer constant ($1/4\pi$) and is found to increase quite rapidly as a function of the temperature. It is remarkable that this regime is observable only within a narrow range of temperatures. At slightly higher temperatures, the curve of the spin stiffness recovers a much more conventional behavior: smooth decrease as a function of the size and cancellation of ρ at some finite lattice size corresponding to some finite correlation length. Regarding the theoretical interpretation of our results, we show that the very low-temperature regime is in full agreement with the RG predictions. The so-called “almost-spin wave” and “vortex” regimes are much more puzzling. However, it is shown that the most salient features induced by the topological defects in these regimes can be rather well reproduced using some simple phenomenological RG equa-

tions which combine the topology of the XY model and the spin-wave content of the O(4) model.

The organization of the paper is as follows. In Sec. II, the various actions of the lattice models are presented. In Sec. III, the expressions of the spin stiffnesses suitable for Monte Carlo simulations are given. In Sec. IV, we present briefly the Wolff-Swendsen-Wang algorithm used. Our results are given in Sec. V. In this latter section we present the behavior of the spin stiffnesses as a function of the lattice size in the various temperature regimes going from low to high temperatures. Finally, we present in the last section our first attempt toward a theoretical interpretation of the effect of the vortices in the almost-spin-wave and vortex regimes.

II. THE LATTICE MODELS

A. The SO(3) \otimes O(2) top model

Our first step is to map the HAFT model into an equivalent nonfrustrated one. As shown by Dombre and Read¹⁹ and Azaria *et al.*²⁰ the long-distance effective Hamiltonian of the HAFT model consists in a system of classical interacting tops. This can be understood from the fact that the 120° structure of the spins of the HAFT model in the ground state fully breaks the SO(3) symmetry so that the order parameter is a rotation matrix $R \in \text{SO}(3)$, a classical top. As in the nonfrustrated case, once the theory is reformulated in terms of the order parameter, the effective interaction becomes ferromagnetic. The Hamiltonian of the top model thus reads^{19,20}

$$H_1 = - \sum_{\langle i,j \rangle} \text{Tr}(PR_i^{-1}R_j), \quad (2)$$

where R_i is a rotation matrix of SO(3) defined on site i and $P = \text{diag}(p_1, p_1, p_3)$ is a diagonal matrix of positive coupling constants which represents the interaction strengths between the different axes of the tops. Note that the temperature has been included in the p_i 's. The HAFT model corresponds to the special case $p_3 = 0$.^{19,20} The SO(3) symmetry of the HAFT is realized here through the rotational invariance of Hamiltonian (2) under left global SO(3) rotations $R_i \rightarrow UR_i$, $U \in \text{SO}(3)$. With the matrix P considered here it is also invariant under the O(2) group of right global transformations: $R_i \rightarrow R_iV$ that commute with the matrix P . Thus, Hamiltonian (2) is invariant under the group $G = \text{SO}(3) \otimes \text{O}(2)$. This left O(2) group is reminiscent of the C_{3v} symmetry of the triangular lattice. Note that it will be convenient in the following to consider the case $p_3 \neq 0$ since the Hamiltonian made with this P is the general one invariant under $G = \text{SO}(3) \otimes \text{O}(2)$ and that, as well known,^{20,16} the condition $p_3 = 0$ is not preserved by renormalization.

The symmetry breaking pattern described by Hamiltonian (2) is $G = \text{SO}(3) \otimes \text{O}(2)$ broken down to $H = \text{O}(2)$:

$$\frac{G}{H} = \frac{\text{SO}(3) \otimes \text{O}(2)}{\text{O}(2)} \equiv \text{SO}(3), \quad (3)$$

where the notation \equiv means that G/H is topologically isomorphic to SO(3). The symmetry breaking pattern thus cor-

responds to a fully broken $\text{SO}(3)$ group. For the original HAFT model, this symmetry breaking pattern is $G/H = \text{SO}(3) \otimes C_{3v}/C_{3v}$ and is thus identical to that given by Eq. (2). This is the reason why the substitution of the discrete C_{3v} by the continuous $\text{O}(2)$ one in Hamiltonian (2) is harmless. It is interesting to note the identity $\text{SO}(3) = \text{SO}(4)/[\text{SO}(3) \otimes Z_2] = S_3/Z_2$, S_3 being the three-sphere, since it shows that the model of tops (2) is equivalent to that of four-component spins living on the four-dimensional unit sphere with antipodal points identified. This will allow us, in the following, to build a vector model equivalent to the preceding matrix one and suitable for Monte Carlo simulations. Note finally that when $p_1 = p_3$ the symmetry group is enlarged to $G = \text{SO}(3) \otimes \text{SO}(3)$ and the symmetry breaking pattern is $G/H = \text{SO}(3) \otimes \text{SO}(3)/\text{SO}(3)$.

B. The $\text{SU}(2) \otimes \text{U}(1)$ top model

We now build the topologically trivial counterpart of the previous top model. We want to preserve the spin-wave part of the model while discarding the topological excitations. Since the spin-wave excitations correspond to small fluctuations of the order parameter, they only probe the local structure of the order parameter space G/H and not its global — topological — structure. This local structure is itself completely determined by the Lie algebras of G and H .^{20,21} We thus need a model defined by an order parameter space G'/H' locally isomorphic to G/H and topologically trivial. This is obtained by considering the covering group $\text{SU}(2)$ of $\text{SO}(3)$. The relevant model is thus built on the manifold $\text{SU}(2) \otimes \text{U}(1)/\text{U}(1)$. The most general Hamiltonian invariant under $\text{SU}(2) \otimes \text{U}(1)$ writes

$$H_2 = - \sum_{\langle i,j \rangle} \left\{ 2(p_1 + p_3) \text{Tr} g_i^{-1} g_j + \frac{1}{2}(p_1 - p_3) \times (\text{Tr} \sigma_3 g_i^{-1} g_j)^2 \right\}, \quad (4)$$

where $g_i \in \text{SU}(2)$ and σ_3 is the third Pauli matrix. The first term in this Hamiltonian is clearly invariant under the cross product of a left $\text{SU}(2)$ group and a right $\text{SU}(2)$ group: $g_i \rightarrow M g_i N$, $M, N \in \text{SU}(2)$. The second one explicitly breaks the right $\text{SU}(2)$ down to a right $\text{U}(1)$ so that the Hamiltonian is generically $\text{SU}(2) \otimes \text{U}(1)$ invariant. This $\text{U}(1)$ symmetry corresponds to the $\text{O}(2)$ symmetry of Hamiltonian (2).

The symmetry breaking pattern described by Hamiltonian (4) is $G' = \text{SU}(2) \otimes \text{U}(1)$ broken down to $H' = \text{U}(1)$:

$$\frac{G'}{H'} = \frac{\text{SU}(2) \otimes \text{U}(1)}{\text{U}(1)} \equiv \text{SU}(2) \quad (5)$$

so that it corresponds to a fully broken $\text{SU}(2)$ group. Again, it is interesting for the following to note the identity $\text{SU}(2) = \text{SO}(4)/\text{SO}(3) = S_3$ which means that the model (4) is equivalent to that of four-component spins living on the four-dimensional unit sphere. Again, when $p_1 = p_3$, the symmetry group is enlarged to $G' = \text{SU}(2) \otimes \text{SU}(2)$ and the symmetry breaking pattern becomes $\text{SU}(2) \otimes \text{SU}(2)/\text{SU}(2)$. Note finally

that the choice of coupling constants in Eq. (4) is such that the two models (2) and (4) have the same temperature scale.

The models corresponding to Eqs. (2) and (4) have, by construction, the same spin-wave dynamics but can nevertheless strongly differ when excitations associated with the topology are activated. The $\text{SU}(2) \otimes \text{U}(1)$ model being topologically trivial, i.e., $\pi_1[\text{SU}(2)] = 0$, we expect that a Monte Carlo study of this model will be well reproduced by a pure spin-wave approach. We show in the following that this is indeed what happens: as in the topologically trivial $\text{O}(N)/\text{O}(N-1)$ ferromagnetic spin systems, the critical properties of the $\text{SU}(2) \otimes \text{U}(1)$ model are in perfect agreement with the perturbative RG predictions made on the continuous limit of the top model, a $\text{NL}\sigma$ model. On the other hand, the $\text{SO}(3) \otimes \text{O}(2)$ model being topologically non-trivial, some disagreement between the perturbative and Monte Carlo approaches at sufficiently high temperatures are found, as expected.

C. The vectorial version of the $\text{SO}(3) \otimes \text{O}(2)$ model

As already mentioned in the Introduction, the cluster algorithms are easier to implement for spins than for matrices. We thus need vectorial versions of our Hamiltonians. This is achieved by using the decomposition of a rotation matrix R_i of $\text{SO}(3)$ in terms of a four-component unit vector $\vec{S}_i = (S_i^0, \mathbf{S}_i) = (S_i^0, S_i^1, S_i^2, S_i^3)$:

$$R_i^{kl} = 2 \left(S_i^k S_i^l - \frac{1}{4} \delta_{kl} \right) + 2 \epsilon_{klm} S_i^0 S_i^m + 2 \left(S_i^{02} - \frac{1}{4} \right) \delta_{kl}. \quad (6)$$

The Hamiltonian (2) then takes the form

$$H'_1 = - \sum_{\langle i,j \rangle} \left\{ 4p_1 \left((\vec{S}_i \cdot \vec{S}_j)^2 - \frac{1}{4} \right) + 4(p_3 - p_1) \times \left[(S_i^0 S_j^0 + S_i^3 S_j^3) (S_i^1 S_j^1 + S_i^2 S_j^2) + (S_i^0 S_j^3 - S_i^3 S_j^0) \times (S_i^1 S_j^2 - S_i^2 S_j^1) + \frac{1}{4} (S_i^{02} + S_i^{32} - S_i^{12} - S_i^{22}) \times (S_j^{02} + S_j^{32} - S_j^{12} - S_j^{22}) \right] \right\}. \quad (7)$$

The first term of Eq. (7) represents the hamiltonian of a system of spherical tops, i.e., $\text{SO}(3) \otimes \text{SO}(3) \approx \text{SO}(4)$ symmetric, for which $p_1 = p_3$. This term is also invariant under a local-gauge- Z_2 group. This Z_2 symmetry expresses the non-trivial topological character of the $\text{SO}(3)$ group. The first term of Eq. (7) is also known as the Hamiltonian of the $RP^3 = \text{SO}(4)/[\text{SO}(3) \otimes Z_2]$ model which expresses the isomorphism between the manifolds $\text{SO}(3)$ and RP^3 . This model and, more generally, the RP^N models for general N have been extensively studied and the question of the nature of their continuum limit²²⁻²⁷ strongly debated, also in connection with topological defects. The second term of Hamiltonian (7) also displays the Z_2 local symmetry but breaks the

global SO(4) symmetry so that the Hamiltonian is generically globally SO(3)⊗O(2) and locally Z₂ symmetric.

D. The vectorial version of the SU(2)⊗U(1) spin model

It is also possible to express Hamiltonian (4) in terms of four-component vectors \vec{S}_i . Using the decomposition of a SU(2) matrix

$$g_i = S_i^0 + i\boldsymbol{\sigma} \cdot \mathbf{S}_i, \quad (8)$$

σ_k , $k=1,2,3$ being the Pauli matrices, Hamiltonian (4) writes

$$H'_2 = - \sum_{\langle i,j \rangle} 4(p_1 + p_3) \vec{S}_i \cdot \vec{S}_j + 2(p_1 - p_3) \times (S_i^0 S_j^3 - S_j^0 S_i^3 - S_i^2 S_j^1 + S_j^2 S_i^1)^2. \quad (9)$$

In this expression the first term is O(4) globally invariant and corresponds to the Hamiltonian of a four-component ferromagnet whereas the second term breaks this symmetry. The Hamiltonian (9) is thus generically globally SU(2)⊗U(1) symmetric. Note that the Z₂ local symmetry has now disappeared. This is a consequence of the trivial topological character of SU(2). Note also that the scale of temperature has been chosen so that both Hamiltonians H'_1 , Eq. (7), and H'_2 , Eq. (9), have the same linearized spin-wave form in the symmetric case ($p_1 = p_3$), namely, $H'_{1/2} = - \sum_{\langle i,j \rangle} 8p_1 \delta \vec{S}_i \cdot \delta \vec{S}_j$ where $\delta \vec{S}$ represents the spin deviation from the reference vector. Finally, remark that the Jacobians resulting from the change of variables: matrices \rightarrow spins in both SO(3)⊗O(2) and SU(2)⊗U(1) are trivial and thus do not contribute to the free energy.

III. THE SPIN STIFFNESSES

A. The spin stiffnesses of the lattice models

The spin stiffness ρ_α to be computed numerically is defined as the free energy increment under twisting the boundary conditions, for instance in the x direction around the direction α . This is realized by coupling the system with two walls of tops $R(x=0) = R_1$ and $R(x=L) = R_2$, R_2 being deduced from R_1 by a rotation of angle θ_α around the direction α and by measuring the variation of the free energy with respect to θ_α :

$$\rho_\alpha = \left. \frac{\partial^2 F(\theta_\alpha)}{\partial \theta_\alpha^2} \right|_{\theta_\alpha=0}. \quad (10)$$

For a system with partition function

$$Z = \sum_{[R_i]} e^{-H} \quad (11)$$

we have

$$\rho_\alpha = -T \left[- \left\langle \frac{\partial H}{\partial \theta_\alpha} \right\rangle^2 - \left\langle \frac{\partial^2 H}{\partial \theta_\alpha^2} \right\rangle + \left\langle \left(\frac{\partial H}{\partial \theta_\alpha} \right)^2 \right\rangle \right]_{\theta_\alpha=0}. \quad (12)$$

Since H is even in the θ_α 's, the average value of $\partial H / \partial \theta_\alpha$ is equal to zero and only the two last terms of Eq. (12) need to be computed.

1. The spin stiffnesses of the SO(3)⊗O(2) model

In principle we have to compute the different average values in Eq. (12) from the partition function

$$Z = \sum_{[R_i]} \exp \left(\sum_{\langle i,j \rangle} \text{Tr} P R_i^{-1} R_j \right) \quad (13)$$

constrained by the boundary conditions

$$R(x=0) = R_0,$$

$$R(x=L) = R_0 e^{i\theta_\alpha T_\alpha}, \quad (14)$$

where R_0 is a rotation matrix of reference (e.g., $R_0 = \mathbb{1}$), T_α is the generator of rotation around the α direction, and θ_α the angle of rotation [Eq. (14) must be understood *without* the sum over α]. However, in practice, the presence of derivatives with respect to θ_α in Eq. (12) as well as the fact that the cluster algorithm is implemented with spins, makes expression (12) not suitable for our simulations. We proceed in two steps to reformulate the model in a numerically convenient way. First, to get rid of the derivatives, we compute them analytically and rewrite the average values in Eq. (12) as θ_α -independent quantities. To do this we decompose R_i into a zero temperature part R_i^{cl} and a fluctuation part h_i :

$$R_i = R_i^{cl} h_i, \quad (15)$$

where both R_i^{cl} and h_i belong to SO(3). In Eq. (15), R_i^{cl} is by definition a solution of the classical equations of motion and thus reads

$$R_i^{cl} = e^{-i\theta_\alpha T_\alpha(x_i/L)} \quad (16)$$

and the h_i 's satisfy the boundary conditions

$$h(x=0) = h(x=L) = \mathbb{1}. \quad (17)$$

We thus have

$$\left. \frac{\partial H}{\partial \theta_\alpha} \right|_{\theta_\alpha=0} = \frac{1}{L} \sum_{\langle i,j \rangle, k,l,m} p_k \epsilon_{\alpha lm} h_i^{kl} h_j^{km} (x_i - x_j),$$

$$\left. \frac{\partial^2 H}{\partial \theta_\alpha^2} \right|_{\theta_\alpha=0} = \frac{1}{L^2} \sum_{\langle i,j \rangle, k,l,m} p_k [\delta_{lm} h_i^{kl} h_j^{km} - h_i^{k\alpha} h_j^{k\alpha}] (x_i - x_j)^2. \quad (18)$$

The average values in Eq. (12) must now be computed with

$$Z = \sum_{[h_i]} \exp \left(\sum_{\langle i,j \rangle} \text{Tr} P h_i^{-1} h_j \right) \quad (19)$$

with the boundary conditions (17). At this stage, everything is written in terms of the h 's. Thus we can now perform the second step of our derivation that consists in using in Eqs. (17), (18) and (19) the same decomposition as in Eq. (6) but now for the h_i 's

$$h_i^{kl} = 2 \left(S_i^k S_i^l - \frac{1}{4} \delta_{kl} \right) + 2 \epsilon_{klm} S_i^0 S_i^m + 2 \left(S_i^{02} - \frac{1}{4} \right) \delta_{kl}. \quad (20)$$

Since now all thermal average values are entirely expressed in terms of four-component spins, the cluster algorithm can be implemented to compute the spin stiffnesses.

2. The spin-stiffnesses of the $SU(2) \otimes U(1)$ model

The same method can be employed for the $SU(2) \otimes U(1)$ model for which we have

$$Z = \sum_{\{g_i\}} \exp \left(\sum_{\langle i,j \rangle} 2(p_1 + p_3) \text{Tr} g_i^{-1} g_j + \frac{1}{2} (p_1 - p_3) \times (\text{Tr} \sigma_3 g_i^{-1} g_j)^2 \right) \quad (21)$$

with, again, the fixed boundary conditions

$$g(x=0) = g_0,$$

$$g(x=L) = g_0 e^{i\theta_\alpha (\sigma_\alpha / 2)}, \quad (22)$$

where g_0 is a rotation matrix of reference of $SU(2)$ (e.g., $g_0 = 1$), σ_α is a Pauli matrix, and θ_α the angle of rotation [again in Eq. (22) there is no sum over α].

As in the $SO(3)$ case, we make the decomposition in classical and fluctuating parts

$$g_i = g_i^{cl} h_i \quad (23)$$

with

$$g_i^{cl} = e^{i\theta_\alpha (\sigma_\alpha / 2) (x_i / L)} \quad (24)$$

and h satisfying

$$h(x=0) = h(x=L) = 1. \quad (25)$$

The different terms of Eq. (12) are separated into $SO(4)$ and $SU(2) \otimes U(1)$ symmetric parts. Writing $S = S_{SO(4)} + S_{SU(2) \otimes U(1)}$ and using the decomposition

$$h_i = S_i^0 + i \boldsymbol{\sigma} \cdot \mathbf{S}_i, \quad (26)$$

we have with obvious notations

$$\left. \frac{\partial H_{O(4)}}{\partial \begin{pmatrix} \theta_1 \\ \theta_2 \\ \theta_3 \end{pmatrix}} \right|_{\theta_\alpha=0} = \frac{2}{L} (p_1 + p_3) \sum_{\langle i,j \rangle} \begin{pmatrix} S_i^0 S_j^1 - S_i^1 S_j^0 + S_i^3 S_j^2 - S_i^2 S_j^3 \\ S_i^0 S_j^2 - S_i^2 S_j^0 + S_i^1 S_j^3 - S_i^3 S_j^1 \\ S_i^0 S_j^3 - S_i^3 S_j^0 + S_i^2 S_j^1 - S_i^1 S_j^2 \end{pmatrix} (x_j - x_i),$$

$$\left. \frac{\partial H_{SU(2) \otimes U(1)}}{\partial \begin{pmatrix} \theta_1 \\ \theta_2 \\ \theta_3 \end{pmatrix}} \right|_{\theta_\alpha=0} = \frac{2}{L} (p_3 - p_1) \sum_{\langle i,j \rangle} \omega_{ij}^3 \begin{pmatrix} S_i^3 S_j^1 + S_i^1 S_j^3 - S_i^2 S_j^0 - S_i^0 S_j^2 \\ S_i^3 S_j^2 + S_i^2 S_j^3 + S_i^1 S_j^0 + S_i^0 S_j^1 \\ S_i^0 S_j^0 + S_i^3 S_j^3 - S_i^1 S_j^1 - S_i^2 S_j^2 \end{pmatrix} (x_j - x_i),$$

$$\left. \frac{\partial^2 H_{O(4)}}{\partial \begin{pmatrix} \theta_1^2 \\ \theta_2^2 \\ \theta_3^2 \end{pmatrix}} \right|_{\theta_\alpha=0} = \frac{1}{L^2} (p_1 + p_3) \sum_{\langle i,j \rangle} \begin{pmatrix} \vec{S}_i \cdot \vec{S}_j \\ \vec{S}_i \cdot \vec{S}_j \\ \vec{S}_i \cdot \vec{S}_j \end{pmatrix} (x_j - x_i)^2,$$

$$\left. \frac{\partial^2 H_{SU(2) \otimes U(1)}}{\partial \begin{pmatrix} \theta_1^2 \\ \theta_2^2 \\ \theta_3^2 \end{pmatrix}} \right|_{\theta_\alpha=0} = \frac{1}{L^2} (p_1 - p_3) \sum_{\langle i,j \rangle} \begin{pmatrix} (S_i^3 S_j^1 + S_i^1 S_j^3 - S_i^2 S_j^0 - S_i^0 S_j^2)^2 - \omega_{ij}^{3,2} \\ (S_i^3 S_j^2 + S_i^2 S_j^3 + S_i^1 S_j^0 + S_i^0 S_j^1)^2 - \omega_{ij}^{3,2} \\ (S_i^0 S_j^0 + S_i^3 S_j^3 - S_i^1 S_j^1 - S_i^2 S_j^2)^2 - \omega_{ij}^{3,2} \end{pmatrix} (x_j - x_i)^2, \quad (27)$$

with

$$\omega_{ij}^3 = -S_i^0 S_j^3 + S_i^3 S_j^0 - S_i^1 S_j^2 + S_i^2 S_j^1. \quad (28)$$

The spin stiffnesses can now be computed with

$$Z = \sum_{\{h_i\}} \exp \left(\sum_{\langle i,j \rangle} 2(p_1 + p_3) \text{Tr} h_i^{-1} h_j + \frac{1}{2}(p_1 - p_3) \times (\text{Tr} \sigma_3 h_i^{-1} h_j)^2 \right) \quad (29)$$

with the set of equations (27) and the boundary conditions (25) or, in terms of the four-component vector \vec{S} :

$$\vec{S}(x=0) = \vec{S}(x=L) = (1,0,0,0). \quad (30)$$

B. The spin-stiffnesses of the NL σ models

The spin stiffnesses can be analytically computed from the continuum versions of the top models, which is a nonlinear sigma (NL σ) model. They identify with the effective coupling constants of the NL σ model at scale L , renormalized by thermal fluctuations. Let us recall that the perturbative treatment of the NL σ model takes only into account the spin-wave part of the spin stiffnesses. Indeed, the β functions of any NL σ model are completely determined by the local properties, i.e., by the metric, of the manifold G/H while they are insensitive to its global, i.e., topological, structure. Since the metric itself is completely determined by the Lie algebras of G and H , the perturbative β functions — and thus the behavior of the spin-wave part of the spin stiffnesses — of the $\text{SO}(3) \otimes \text{O}(2)$ and $\text{SU}(2) \otimes \text{U}(1)$ NL σ models are identical by construction. They are given at two-loop order by^{20,16}

$$\begin{aligned} \frac{\partial \tilde{\rho}_1(l)}{\partial l} &= -\frac{1}{2\pi} + \frac{1}{4\pi} \frac{\tilde{\rho}_3(l)}{\tilde{\rho}_1(l)} - \frac{5}{32\pi^2} \frac{\tilde{\rho}_3(l)^2}{\tilde{\rho}_1(l)^3} + \frac{3}{8\pi^2} \frac{\tilde{\rho}_3(l)}{\tilde{\rho}_1(l)^2} \\ &\quad - \frac{1}{4\pi^2 \tilde{\rho}_1(l)}, \\ \frac{\partial \tilde{\rho}_3(l)}{\partial l} &= -\frac{1}{4\pi} \frac{\tilde{\rho}_3(l)^2}{\tilde{\rho}_1(l)^2} - \frac{1}{32\pi^2} \frac{\tilde{\rho}_3(l)^3}{\tilde{\rho}_1(l)^4}, \end{aligned} \quad (31)$$

with $l = \ln L/a$ where L is the system size, a the lattice spacing, the initial conditions of the RG flow being given by

$$\begin{aligned} \tilde{\rho}_1(l=0) &= p_1 + p_3, \\ \tilde{\rho}_3(l=0) &= 2p_1. \end{aligned} \quad (32)$$

Note that the RG equations (31) are written in terms of quantities that contain, in their definition, the temperature, as it is clear from Eq. (32) since the temperature is included in the p_i 's. The Monte Carlo counterpart of the $\tilde{\rho}_\alpha$'s are thus given by the ρ_α/T 's previously defined.

In contrast with the O(N) case, there are *a priori* three different spin stiffnesses in our case but, in fact, only two are

independent since the left O(2) symmetry constrains two of them to be identical. Note that, asymptotically, i.e., for $L \gg a$, the behavior of the $\tilde{\rho}_\alpha$'s is given by the infrared limit of the flow equations. It is easy to show that, in this limit $\tilde{\rho}_1 \rightarrow \tilde{\rho}_3$ and the model becomes effectively $\text{SO}(3) \otimes \text{SO}(3) \sim \text{SO}(4)$ symmetric. This is the known phenomenon of enlarged symmetry.^{4,20} We recover therefore the universal scaling of the spin stiffness of a ferromagnetic $N=4$ vector model. At leading order we have¹⁶

$$\tilde{\rho}_1 \sim \tilde{\rho}_3 \sim \frac{1}{4\pi} \ln \frac{\xi}{L}, \quad (33)$$

where ξ is the correlation length. Note, of course, that since the spin stiffnesses in Eq.(31) are calculated perturbatively, they can only be valid in a limited range of *low* temperatures where the perturbation theory at two-loop order is meaningful.

From the preceding analysis, it should be clear that for a topologically trivial model, the spin-wave part of the spin stiffness $\tilde{\rho}_\alpha$ identifies with ρ_α/T , so that we can expect that this last quantity follows the RG equations calculated by perturbation theory. Indeed, for the $O(N)$ model, it has been checked²⁸ that at sufficiently low temperature, the spin stiffness ρ_α/T follows the RG equations calculated by means of the $O(N)$ NL σ model up to two loop order.^{29,15} In the same way, we expect the different spin stiffnesses ρ_α/T of the lattice $\text{SU}(2) \otimes \text{U}(1)$ model calculated by Monte Carlo simulation to follow the RG equations (31) in a large range of low temperatures since it is topologically trivial. On the other hand, we expect the behavior of the spin stiffnesses ρ_α/T of the lattice $\text{SO}(3) \otimes \text{O}(2)$ model to agree with Eq. (31) at very low temperature, i.e., below T_V , where the topological defects are not activated, but to disagree with the perturbative RG predictions near and above the crossover temperature T_V .

IV. WOLFF-SWENDSEN-WANG ALGORITHM

The simulations presented in this paper are based on a generalization of the Wolff-Swendsen-Wang^{17,18,30,31} algorithm to N -vector models as presented by Caracciolo *et al.* in Ref. 32. The method is based on an embedding of Ising spins ϵ into the N component (here $N=4$) continuous spins \vec{S} according to

$$\vec{S}_i = \vec{S}_i^\perp + \epsilon_i |\vec{S}_i^\parallel| \vec{r}, \quad (34)$$

where \vec{r} is a unit vector chosen randomly on the sphere S^3 , $\vec{S}_i^\perp = \vec{S}_i - (\vec{S}_i \cdot \vec{r}) \vec{r}$ and $\vec{S}_i^\parallel = (\vec{S}_i \cdot \vec{r}) \vec{r}$ are the components of the spin vector perpendicular and parallel to the unit vector \vec{r} , the Ising variable ϵ_i being given by $\epsilon_i = \text{sgn}(\vec{S}_i \cdot \vec{r}) = \pm 1$. Once this embedding is done, our initial Hamiltonian written in terms of continuous spins — here, Hamiltonians (7) and (9) — can be rewritten as a generalized random-bond Ising model. In the Monte Carlo simulation the spin variables of this new problem are updated using an efficient nonlocal algorithm for Ising variables (e.g., the standard Swendsen-Wang algorithm). To flip the Ising variable ϵ_i corresponds to

make a reflection of the vector \vec{S}_i in the hyperplane perpendicular to \vec{r} . A necessary condition to get an efficient Wolff-type algorithm is that this transformation preserves the total energy of the system. In that case its application to a large set of spins costs only a surface energy and large-scale changes in the spin configuration are possible. Here, such a condition is verified only for the symmetric part ($p_1=p_3$) of the Hamiltonians. As a consequence, we have chosen to perform our simulations with the reference symmetric Hamiltonians. More precisely, for the $\text{SO}(3)\otimes\text{O}(2)$ model we consider

$$H^{(0)} = - \sum_{\langle i,j \rangle} 4p_1 \left((\vec{S}_i \cdot \vec{S}_j)^2 - \frac{1}{4} \right) \quad (35)$$

and for the $\text{SU}(2)\otimes\text{U}(1)$ model we take

$$H^{(0)} = - \sum_{\langle i,j \rangle} 8p_1 \vec{S}_i \cdot \vec{S}_j. \quad (36)$$

Note that both Hamiltonians reduce to the same Hamiltonian in the spin-wave approximation ($H_{\text{SW}} = - \sum_{\langle i,j \rangle} 8p_1 \delta\vec{S}_i \cdot \delta\vec{S}_j$ where $\delta\vec{S}$ represents the spin deviation from the reference vector). Note also that the zero-temperature ground-state energies are different for the two Hamiltonians. This is not important since the various quantities computed in this work do not depend on this reference energy.

Calculation of exact properties associated with the full Hamiltonians are done by reweighting appropriately the Monte Carlo averages. Let us write \bar{Q} the average of an arbitrary function $Q(S)$ of the spin configuration S

$$\bar{Q} = \int d\vec{S}_1 \dots \int d\vec{S}_M Q(S) e^{-H(S)/T} / Z, \quad (37)$$

where M is the total number of spins considered, $H(S)$ is the exact Hamiltonian, and Z the partition function. We reexpress \bar{Q} as follows:

$$\begin{aligned} \bar{Q} &= \int d\vec{S}_1 \dots \int d\vec{S}_M Q(S) e^{-V(S)/T} \\ &\times e^{-H^{(0)}(S)/T} \\ &\int d\vec{S}_1 \dots \int d\vec{S}_M e^{-V(S)/T} \\ &\times e^{-H^{(0)}(S)/T}, \end{aligned} \quad (38)$$

where V is the difference between the exact and reference Hamiltonian $V \equiv H - H^{(0)}$. The Monte Carlo averages are performed over the set of spin configurations distributed according to the Boltzmann weight associated with the reference Hamiltonian (denoted here as $\langle\langle \dots \rangle\rangle_0$)

$$\bar{Q} = \langle\langle Q(S) e^{-V(S)/T} \rangle\rangle_0 / \langle\langle e^{-V(S)/T} \rangle\rangle_0. \quad (39)$$

By using such a procedure we are sure that at the symmetric point ($p_1=p_3$) our simulations are free from the critical slowing down problem (see, Ref. 32). Away from the symmetric point, the situation is less clear. There is a subtle

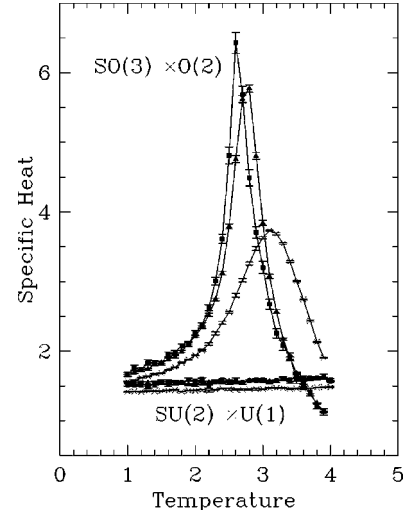


FIG. 1. Specific heat as a function of the temperature for the $\text{SO}(3)\otimes\text{O}(2)$ and $\text{SU}(2)\otimes\text{U}(1)$ models. Three different sizes have been considered: 4×4 (crosses), 10×10 (solid triangles), and 20×20 (solid squares). For the $\text{SU}(2)\otimes\text{U}(1)$ case the curves corresponding to the two largest sizes are undistinguishable.

interplay between the loss due to the undesirable fluctuations of the weight in averages (a growing source as the asymmetric parameter $\Delta p \equiv p_1 - p_3$ is increased) and the gain obtained from the treatment of the large-scale collective-mode moves issued from the reference Hamiltonian. In practice, we have found that realistic calculations can be done only for a small value of Δp with a maximum value of about 0.2. Although we have not made a systematic study of the effective (associated with H and not $H^{(0)}$) dynamical exponent, we are quite confident that, in the regime $\Delta p < 0.2$, the convergence of the estimators at the very low temperatures we have considered is very satisfactory. In order to compute the spin stiffnesses we have used formulas (12), (18), and (27) presented in the previous section.

V. MONTE CARLO RESULTS

In this section we present the calculations of the spin stiffnesses for the $\text{SO}(3)\otimes\text{O}(2)$ and $\text{SU}(2)\otimes\text{U}(1)$ models. Before that, let us first give a qualitative visualization of the effect of topology in this problem. Figure 1 presents the specific heat as a function of the temperature for the two models and for three different lattice sizes: 4×4 , 10×10 , and 20×20 . Already for these relatively small systems the effect of topology is striking. In the $\text{SO}(3)\otimes\text{O}(2)$ case, the specific heat curves show a marked maximum whereas it is not the case for the topologically trivial $\text{SU}(2)\otimes\text{U}(1)$ model. This maximum is usually interpreted as the signature of the presence of topological excitations. Note that the location of the maximum provides a rough estimate of the crossover temperature at which these excitations are activated.⁸ Here, and without making a detailed analysis based on much bigger sizes, we get approximately $T_V \sim 2.6$. From our numerical results we propose to distinguish four different temperature regimes.

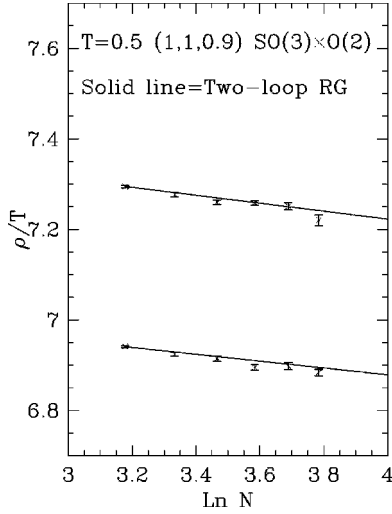


FIG. 2. $SO(3)\otimes O(2)$ spin stiffnesses ρ_1/T (lower curve) and ρ_3/T (upper curve) as a function of $\ln L$. Temperature $T=0.5$ and $(p_1, p_1, p_3)=(1,1,0.9)$. The solid line is the two-loop RG prediction as given by Eq. (31). Open boundary conditions. Number of clusters used ranges from 5×10^6 to 8×10^6 .

A. The spin-wave regime

The spin-wave regime corresponds to the very-low-temperature regime. We have plotted in Figs. 2 and 3 the spin stiffnesses ρ_1/T and ρ_3/T as functions of $\ln L$ at temperature $T=0.5$ for the $SO(3)\otimes O(2)$ and $SU(2)\otimes U(1)$ models, respectively. The parameters of the action are $(p_1, p_1, p_3)=(1,1,0.9)$. The behaviors of the spin stiffnesses of both models are in full agreement with the two-loop RG predictions (solid line), Eq. (31). As expected from our estimate of T_V , these results show that at $T=0.5$ the topological excitations are not yet activated and that the physics is controlled by spin waves well described by the perturbative

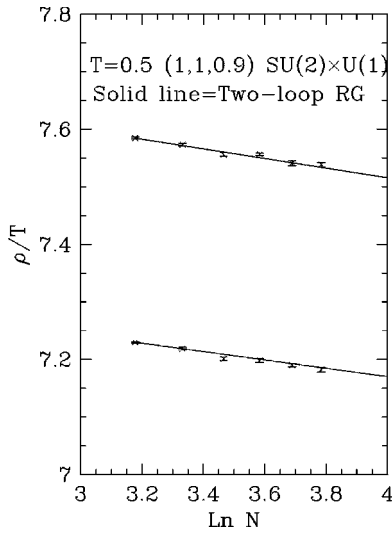


FIG. 3. $SU(2)\otimes U(1)$ spin stiffnesses ρ_1/T (lower curve) and ρ_3/T (upper curve) as a function of $\ln L$. Temperature $T=0.5$ and $(p_1, p_1, p_3)=(1,1,0.9)$. The solid line is the two-loop RG prediction as given by Eq. (31). Open boundary conditions. Number of clusters ranges from 2×10^6 to 4×10^6 .

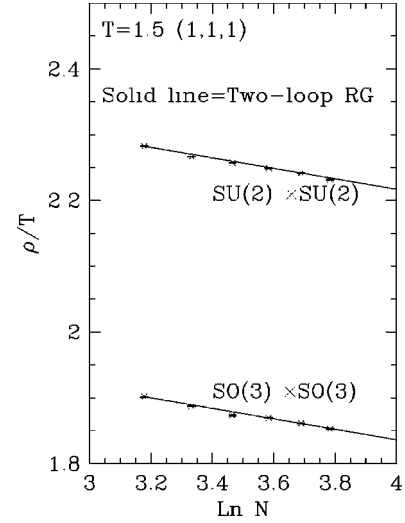


FIG. 4. Spin stiffness as a function of $\ln L$ at $T=1.5$ for the two models in the symmetric case ($p_1=p_3$). Note that in this case all three spin stiffnesses are equal.

$NL\sigma$ model. For this temperature and for the parameters p_1 and p_3 chosen, we find an almost linear behavior as a function of the logarithm of the size. In other words, the two-loop effects are almost negligible. The numerical slopes are fully compatible with the theoretical slope of $1/4\pi$ as given by the one-loop equation (33). Note that, by measuring the two independent spin stiffnesses of the HAFT model, Southern and Young⁹ had already confirmed, for one value of the temperature, the RG predictions.

This overall behavior persists up to temperatures of order $T\sim 1$ where we enter a new regime. Finally, note that the absolute values of the temperature-rescaled spin stiffnesses for the two models at $T=0.5$ are different. Between $T=0$ and $T\sim 1$ this difference is almost constant. At $T=0$, this constant can be calculated analytically, on the lattice models, from the finite parts of the one-loop counterterms that renormalize the couplings. It is found to be equal to $5/16$.

B. The almost-spin-wave regime

For $T\approx 1$, the spin stiffnesses of the two models start to differ: whereas their variations as a function of $\ln L$ are correctly described by Eq. (31) (see Fig. 4) the absolute values of ρ_1/T and ρ_3/T for the $SO(3)\otimes O(2)$ model get smaller and smaller compared to those of the $SU(2)\otimes U(1)$ model as the temperature increases. We have decided to refer to this regime as the almost-spin-wave regime.

Let us now give a quantitative account of this phenomenon. Since the difference between ρ_1/T and ρ_3/T turns out to be irrelevant for this discussion, we restrict ourselves from now on to the fully symmetric $SO(3)\otimes SO(3)$ and $SU(2)\otimes SU(2)$ models where all three spin stiffnesses are equal. The important point is that in the almost-spin-wave regime, the spin stiffness still displays a linear behavior as the function of $\ln L$ even for the topologically nontrivial model. It is thus natural to define a characteristic length ξ_{eff} as:

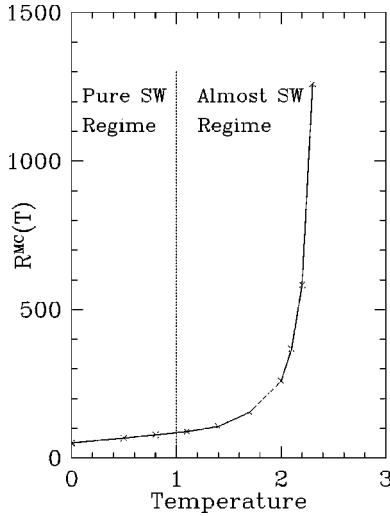


FIG. 5. Ratio of correlation lengths as a function of the temperature as defined in the text. The solid line is just to guide the eyes. The separation at $T \sim 1$ between the pure spin-wave (SW) and the almost-spin-wave regimes is rather arbitrary.

$$\rho/T \equiv \frac{1}{4\pi} \ln \frac{\xi_{\text{eff}}}{L} \quad (40)$$

with ξ_{eff} being a function of T only. We recall that in the topologically trivial $SU(2) \otimes SU(2)$ model and at the one-loop approximation, ξ_{eff} is the correlation length [see Eq. (33)]. Thus, the simplest hypothesis is that the ξ_{eff} of the $SO(3) \otimes SO(3)$ model is still, in this regime, proportional to the correlation length. One can thus expect the ratio

$$R^{\text{MC}}(T) \equiv \frac{\xi_{\text{eff}}[SU(2) \otimes SU(2)]}{\xi_{\text{eff}}[SO(3) \otimes SO(3)]} \quad (41)$$

to be a good indicator of the influence of the topology. We give in Fig. 5, $R^{\text{MC}}(T)$ as a function of the temperature.

From this figure, we see that at low temperatures (in the spin-wave regime) $R^{\text{MC}}(T)$ is almost independent of the temperature. Note that at $T=0$ it converges to a value different from one because of the constant shift of $5/16$ between the two temperature-rescaled spin stiffnesses as discussed above. Within the range of temperatures $T \in [1, 2.1]$ the ratio is found to increase extremely rapidly. We have found that the curve can be well fitted using the form

$$R^{\text{MC}}(T) = C \exp \left[\frac{\alpha}{(T - T_c)^\beta} \right]. \quad (42)$$

The ‘‘best’’ values found are $C = 23.52$, $\alpha = 1.655$, $\beta = 0.600$, and $T_c = 2.532$. This clearly indicates that the topologically nontrivial model becomes more disordered than the topologically trivial one at a temperature of order $T_c = 2.5$, a value compatible with that obtained from the peak of the specific heat. Of course, the analytical form chosen in Eq. (42) must be taken with lot of caution. Many different analytical forms could have been used and give similar results.

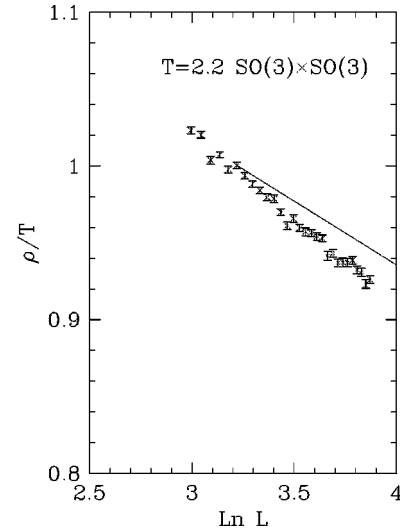


FIG. 6. $SO(3) \otimes SO(3)$ spin stiffness as a function of $\ln L$. $T = 2.2$. The solid line is the two-loop RG prediction.

C. The vortex regime

At temperatures higher than typically $T = 2.1$, we enter in a new regime that we propose to call the vortex regime in which the topological excitations play a major role. Figures 6, 7, 8, and 9 present, for the two models, the spin-stiffness as a function of the size at the temperatures $T = 2.2, 2.4$, and 2.6 , respectively. For the $SU(2) \otimes SU(2)$ model (Fig. 9) the spin stiffness is still correctly described by the two-loop NL σ model predictions Eq. (31). For the $SO(3) \otimes SO(3)$ model it is still possible to define an effective slope at sufficiently small sizes but it now differs significantly from the RG predictions. This effective slope is found to increase as a function of the temperature. For example, at $T = 2.2$ the slope is about ~ -0.115 to be compared with $-1/4\pi \sim -0.080$. At $T = 2.4$ the slope is ~ -0.158 , a value approximately two times larger than in the spin-wave regime. Moreover, the spin stiffness displays some irregularities which could be

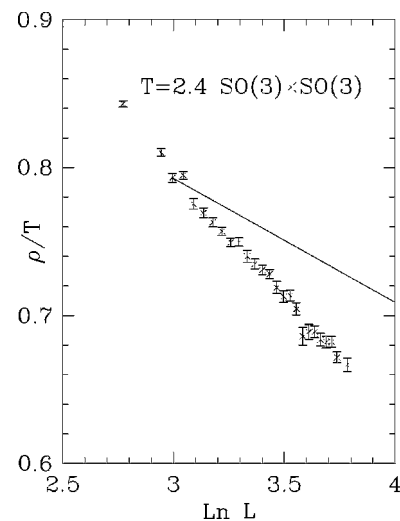


FIG. 7. $SO(3) \otimes SO(3)$ spin stiffness as a function of $\ln L$. $T = 2.4$. The solid line is the two-loop RG prediction.

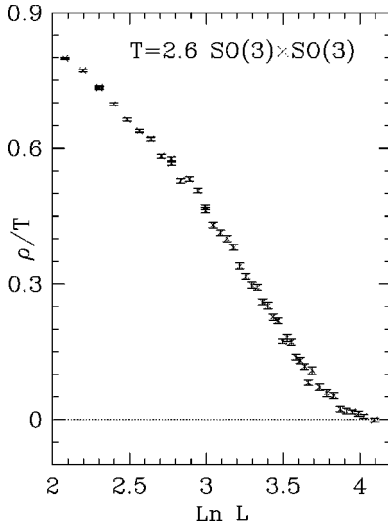


FIG. 8. $SO(3) \otimes SO(3)$ spin-stiffness as a function of $\ln L$. $T = 2.6$.

associated with the presence of long-lived topological configurations that affect the dynamics. The most irregular curve has been obtained at temperature $T = 2.6$ (Fig. 8).

D. The high-temperature regime

At temperatures higher than typically $T = 2.6$ the spin stiffnesses as a function of the size of the $SO(3) \otimes SO(3)$ model recovers a smooth behavior. Figure 10 presents such a behavior at temperature, $T = 2.9$. Figure 11 presents the spin-stiffness for the $SU(2)$ case at $T = 7.7$. The overall behavior of the spin stiffnesses is quite different. In the $SO(3) \otimes SO(3)$ case ρ/T vanishes abruptly with a change of concavity whereas in the $SU(2) \otimes SU(2)$ case it goes slowly down to zero without any change of concavity.

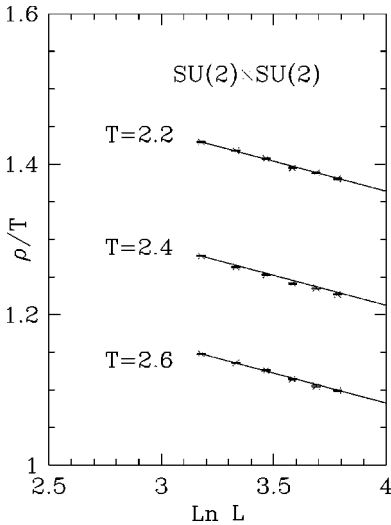


FIG. 9. $SU(2) \otimes SU(2)$ spin stiffnesses as a function of $\ln L$ for $T = 2.2$, $T = 2.4$, and $T = 2.6$. The solid lines are the two-loop RG predictions.

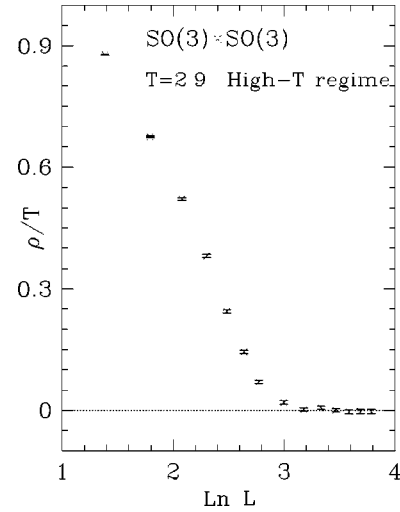


FIG. 10. $SO(3) \otimes SO(3)$ spin-stiffness as a function of $\ln L$. $T = 2.9$. High-temperature regime for the model.

VI. DISCUSSION

We now attempt to give a theoretical analysis of our results. It is notoriously difficult to tackle with the physics of Z_2 topological defects since in this case there is nothing equivalent to the Villain transformation. In the usual ferromagnetic case, $O(N)/O(N-1)$, Cardy and Hamber have proposed to describe the effect of compacity of the sphere S_{N-1} by means of additional terms in the RG equation for the temperature.³³ These equations, valid in the vicinity of $N = 2$ and at order T^3 — which correspond to two-loop in perturbation theory — read³³

$$\frac{dT(l)}{dl} = (N-2) \frac{T(l)^2}{2\pi} + (N-2) \frac{T(l)^3}{(2\pi)^2} + 4\pi^3 y(l)^2 + \dots,$$

$$\frac{dy(l)^2}{dl} = \left(4 - \frac{2\pi}{T(l)}\right) y(l)^2 + \dots. \quad (43)$$

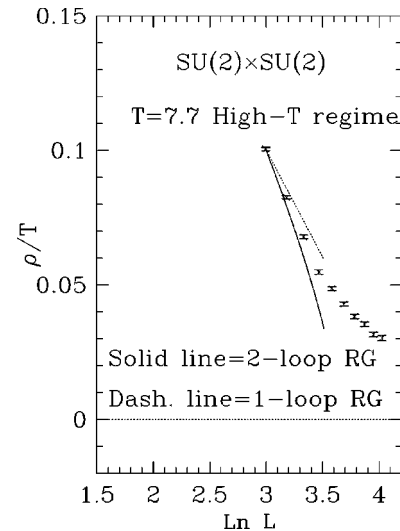


FIG. 11. $SU(2) \otimes SU(2)$ spin-stiffness as a function of $\ln L$. $T = 7.7$. High-temperature regime for the model.

These equations have been derived by assuming analyticity in y^2 and in N and by requiring that the two following limiting cases are recovered: (i) the perturbative β function of the $O(N)$ model for $N \geq 3$; and (ii) the Kosterlitz-Thouless equations for $N=2$. In fact, Cardy and Hamber have shown that it is the only set of equations compatible with these requirements.³³ For $N=2$, one recovers the Kosterlitz-Thouless (KT) equations^{34,35} where y identifies with the fugacity of vortices. The case $y=0$ leads to the two-loop perturbative β function of the $O(N)/O(N-1)$ NL σ model in two dimensions. For $N \neq 2$, y lacks of a clear interpretation but it has been conjectured that it encodes the effect of compacity. Clearly, the ($N > 3$, $y \neq 0$) case we consider here could very well lie outside the domain of validity of these equations. It is therefore important to insist on the fact that they must only be considered as some phenomenological RG equations for a model displaying topological defects, y playing the role of a fugacity by analogy with the KT case. Our aim is to show that they are able to reproduce the gross features of the behavior of the spin stiffness and correlation length found in our case. As in the KT case, the physical ‘‘fugacity’’ $y(l=0)$ that appears as the initial condition in Eq. (43) is not independent on the temperature. However, in contrast with this last case its dependence on the physical temperature $T(l=0)$ is unknown. The simplest assumption we can think of is

$$y(l=0) = e^{-\gamma/T(l=0)} \quad (44)$$

as in the KT case. In Eq. (44), γ is an adjustable parameter.

Equations (43) are considered in the case $N=4$ since $SO(3) \otimes SO(3)/SO(3)$ and $SO(4)/SO(3)$ have the same spin-wave content and differ by their topological properties. These latter properties are expected to be taken into account via the y terms in Eq. (43). Moreover, we write them in terms of the spin stiffness of the $SO(3) \otimes SO(3)/SO(3)$ model. These equations are obtained by the substitution $1/T(l) \rightarrow 4\tilde{\rho}(l)$:

$$\begin{aligned} \frac{d\tilde{\rho}(l)}{dl} &= -\frac{1}{4\pi} - \frac{1}{32\pi^2\tilde{\rho}(l)} - 16\pi^3 y(l)^2 \tilde{\rho}(l)^2, \\ \frac{dy(l)^2}{dl} &= \left(4 - \frac{8\pi}{\tilde{\rho}(l)}\right) y(l)^2. \end{aligned} \quad (45)$$

By direct integration of Eqs. (45) up to the scale L of the lattice size $l = \ln L/a$ one can obtain the dependence of $\tilde{\rho}(l)$ on the temperature $T(l=0)$ and on L . To make contact with our Monte Carlo results, we are also interested in the correlation length ξ . This last quantity is defined, as usual, from the fact that when the RG scale e^l becomes of the order of ξ , the spin stiffness $\tilde{\rho}(l)$ vanishes, see Eq. (40):

$$\xi/a \sim e^l \quad \text{with} \quad \tilde{\rho}(l) \approx 0. \quad (46)$$

As in the Monte Carlo simulations, we compute from Eq. (45) the spin stiffnesses and correlation lengths in both situations: without and with defects. This consists in setting respectively $y(l)$ to zero or not in Eq. (45). Note finally that,

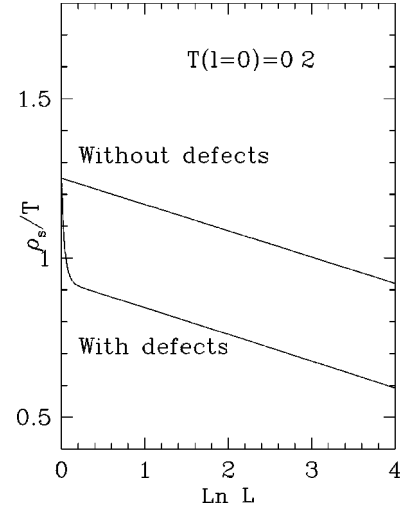


FIG. 12. Spin stiffness as a function of $\ln L$ with and without defects. $T(l=0)=0.2$.

for simplicity, we have chosen to take the same normalization at zero-temperature for the spin stiffnesses with and without defects.

Let us now show that we retrieve the essential features of the regimes previously identified except, obviously, for the high-temperature regime which is out of reach of the RG equations (45) which, for the spin-wave part, are perturbative in the temperature. At very low temperatures, $y(l)$ is very small and remains small along the RG flow. As a result we find almost no difference between the systems with and without vortices: this is the spin-wave regime that we recover trivially.

As the temperature increases, the y -term plays a more and more important role. Adjusting the free parameter γ at a value $\gamma=0.45$ the temperature where the defects start to play a significant role is typically $T(l=0) \sim 0.15$. We plot in Fig. 12 the spin stiffnesses as a function of the system size at a slightly higher temperature $T(l=0)=0.2$. The upper curve corresponds to the system without defects and the lower one to that with defects.

As in our Monte Carlo simulations, we find that the absolute value of the spin stiffness is decreased by the presence of defects. After an abrupt jump at very small sizes the spin stiffness is found to be linear as a function $\ln L$. Up to an accuracy of a few percent, the slope is not affected by the defects. Its value $-0.080 \sim -1/4\pi$, corresponds to the perturbative RG result. This behavior is similar to that predicted by the spin-wave analysis, except that the absolute value of the spin stiffness is smaller. This corresponds to the almost-spin-wave regime previously identified.

To obtain a completely consistent picture, it is also necessary to see whether the ratio of the correlation lengths, without and with defects, considered as a function of $T(l=0)$:

$$R(T) = \frac{\xi_{y(l)=0}}{\xi_{y(l) \neq 0}} \quad (47)$$

behaves as R^{MC} , Fig. 5. We give in Fig. 13, the ratio R obtained by direct integration of Eq. (45). This figure clearly

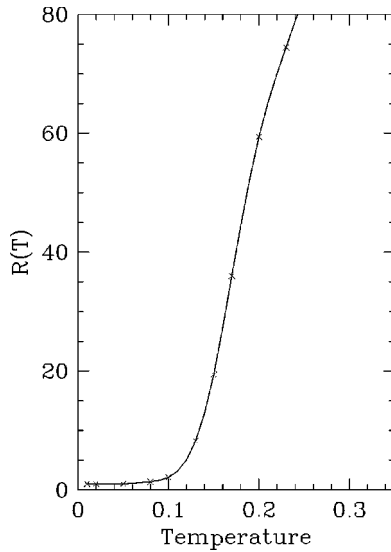


FIG. 13. Ratio $R(T)$ of correlation lengths as a function of $T(l=0)$.

shows a behavior comparable to that observed in Fig. 5.

At higher temperature, one enters in a regime where the spin-stiffness as a function of the size begins to display a different behavior. Figure 14 presents the spin stiffnesses at $T=0.5$ (to facilitate the comparison the dashed line represents the linear behavior associated with the model without defects). It is possible to define a linear regime but now with a slightly greater slope than in the defect-free case. The difference between the two slopes is about 10%. As the temperature is increased the spin-stiffness still displays a linear behavior but now with an increasing temperature-dependent slope.

Such a behavior has been numerically observed in the vortex regime (see, Figs. 6 and 7 where some “effective” linear behavior with a larger slope is observed). However, note that the irregular behavior found in Fig. 8 is not reproduced here. Of course, the range of temperature over which this linear behavior is observed, as well as the variation of the slope with $T(l=0)$ depends rather strongly in our calculation on the relation between $\gamma(l=0)$ and $T(l=0)$, Eq.

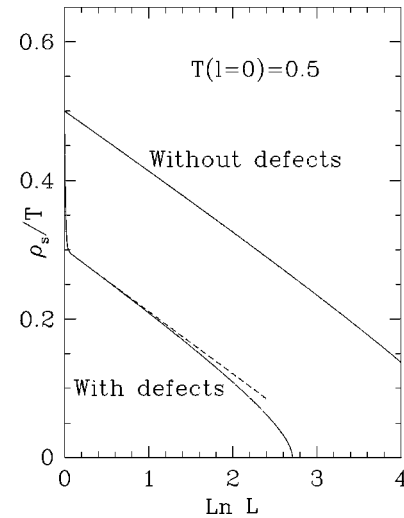


FIG. 14. Spin stiffness as a function of $\ln L$ with and without defects, $T(l=0)=0.5$. The dashed line represents the linear behavior associated with the model without defects. A slight increase of the slope is observed when the defects are present.

(44). With our choice of γ , the maximum variation found for the slope as a function of the temperature is about 15% which is somewhat below what is obtained in the simulations. This could certainly be corrected by another choice of $\gamma(T)$.

At even higher temperature, Eqs. (45) are no longer valid since they are based on a low-temperature expansion and the comparison with the numerical results does not make sense. The preceding analysis shows that the simple set of equations (45) together with the relation (44) seem to capture some of the important features of the presence of topological defects in the almost-spin-wave and vortex regimes. Of course, only a microscopical approach of the problem could allow to go beyond this semiquantitative description.

ACKNOWLEDGMENTS

B.D. and D.M. thank B. Douçot and J. Vidal for discussions. LCT, LPTL, and LPTHE are Laboratoires associés au CNRS: UMR 7676, 7600, and 7589.

¹D. Bailin, A. Love, and M. Moore, *J. Phys. C* **10**, 1159 (1977).

²T. Garel and P. Pfeuty, *J. Phys. C* **L9**, 245 (1976).

³H. Kawamura, *J. Appl. Phys.* **63**, 3086 (1988).

⁴P. Azaria, B. Delamotte, and T. Jolicœur, *Phys. Rev. Lett.* **64**, 3175 (1990).

⁵H. Kawamura, *J. Phys.: Condens. Matter* **10**, 4707 (1998).

⁶M. Tissier, D. Mouhanna, and B. Delamotte, *Phys. Rev. B* **61**, 15 327 (2000).

⁷M. Tissier, B. Delamotte, and D. Mouhanna, *Phys. Rev. Lett.* **84**, 5208 (2000).

⁸H. Kawamura and S. Miyashita, *J. Phys. Soc. Jpn.* **53**, 4138 (1984).

⁹B. Southern and A. Young, *Phys. Rev. B* **48**, 13 170 (1993).

¹⁰B. W. Southern and H-J. Xu, *Phys. Rev. B* **52**, R3836 (1995).

¹¹M. Wintel, H. Everts, and W. Apel, *Europhys. Lett.* **25**, 711 (1994).

¹²W. Stephan and W. Southern, *Phys. Rev. B* **61**, 11 514 (2000).

¹³W. Stephan and W. Southern, cond-mat/0009115 (unpublished).

¹⁴L. Capriotti, R. Vaia, A. Cucoli, and V. Tognetti, *Phys. Rev. B* **58**, 273 (1998).

¹⁵S. Chakravarty, *Phys. Rev. Lett.* **66**, 481 (1991).

¹⁶P. Azaria, B. Delamotte, T. Jolicœur, and D. Mouhanna, *Phys. Rev. B* **45**, 12 612 (1992).

¹⁷R. Swendsen and J. Wang, *Phys. Rev. Lett.* **58**, 86 (1987).

¹⁸U. Wolff, *Phys. Rev. Lett.* **62**, 361 (1989).

¹⁹T. Dombre and N. Read, *Phys. Rev. B* **39**, 6797 (1989).

- ²⁰P. Azaria, B. Delamotte, F. Delduc, and T. Jolicoeur, Nucl. Phys. B **408**, 485 (1993).
- ²¹D. Friedan, Ann. Phys. (N.Y.) **163**, 318 (1985).
- ²²H. Kunz and G. Zumbach, Phys. Rev. B **46**, 662 (1992).
- ²³S. Caracciolo, R. Edwards, A. Pelissetto, and A. Sokal, Phys. Rev. Lett. **71**, 3906 (1993).
- ²⁴M. Hasenbusch and R. Horgan, Phys. Rev. D **53**, 5075 (1996).
- ²⁵M. Hasenbusch, Phys. Rev. D **53**, 3445 (1996).
- ²⁶F. Niedermayer, P. Weisz, and D. Shin, Phys. Rev. D **53**, 5075 (1996).
- ²⁷S. Catteral, M. Hasenbusch, R. Horgan, and R. Renken, Phys. Rev. D **98**, 74 510 (1998).
- ²⁸M. Caffarel, P. Azaria, B. Delamotte, and D. Mouhanna, Europhys. Lett. **26**, 493 (1994).
- ²⁹E. Brézin, E. Korutcheva, T. Jolicoeur, and J. Zinn-Justin, J. Stat. Phys. **70**, 583 (1993).
- ³⁰U. Wolff, Nucl. Phys. B **322**, 759 (1989).
- ³¹U. Wolff, Nucl. Phys. B **334**, 581 (1990).
- ³²S. Caracciolo, R. Edwards, A. Pelissetto, and A. Sokal, Nucl. Phys. B **403**, 475 (1993).
- ³³J. Cardy and H. Hamber, Phys. Rev. Lett. **45**, 499 (1980).
- ³⁴J. Kosterlitz and D. Thouless, J. Phys. C **6**, 97 (1973).
- ³⁵J. Kosterlitz, J. Phys. C **7**, 1046 (1974).